

Regular article

Thermal conductivity of ultrathin BaTiO₃ films grown by plasma-assisted atomic layer depositionJungwan Cho^{a,*}, Joonsuk Park^b, Fritz B. Prinz^{b,c}, Jihwan An^{c,d,**}^a Department of Mechanical Engineering, Kyung Hee University, 1732 Deogyong-daero, Giheung-gu, Yongin-si, Gyeonggi-do 17104, Republic of Korea^b Department of Materials Science and Engineering, Stanford University, Stanford, CA 94305, United States^c Department of Mechanical Engineering, Stanford University, Stanford, CA 94305, United States^d Department of Manufacturing Systems and Design Engineering, Seoul National University of Science and Technology (SeoulTech), Seoul 01811, Republic of Korea

ARTICLE INFO

Article history:

Received 28 March 2018

Received in revised form 9 May 2018

Accepted 29 May 2018

Available online 15 June 2018

Keywords:

High-dielectric-constant thin films

Barium titanate (BaTiO₃)

Atomic layer deposition

Thermal conductivity

Remote plasma

ABSTRACT

We report the first measurements of the room temperature thermal conductivity of ultrathin (12 and 24 nm) barium titanate (BaTiO₃) films prepared by plasma-enhanced atomic layer deposition (PEALD). The measured thermal conductivities of as-deposited films are relatively low as compared to values reported previously. We further investigate the effects of a post-deposition remote oxygen plasma treatment on the crystallinity and thermal conductivity of our PEALD BaTiO₃ films. We find that the thermal conductivity slightly decreases with increasing duration of plasma treatment, which is most likely due to increased phonon scattering at interfaces between amorphous and crystalline phases within the films.

© 2018 Acta Materialia Inc. Published by Elsevier Ltd. All rights reserved.

High-dielectric-constant materials are essential for information storage devices, such as dynamic random access memory (DRAM) [1]. As the individual feature size of the device rapidly shrinks, i.e., the packing density increases, there have been needs for next-generation materials with higher dielectric constants than the current materials of choice (e.g., ZrO₂, HfO₂) [2]. Perovskite-type dielectrics such as BaTiO₃ (BTO), SrTiO₃ (STO), or (Ba,Sr)TiO₃ (BST) have been reported to possess exceptionally high dielectric constants (>100) even in thin films [3–6], and therefore have attracted much attention. Their exotic dielectric properties are known to be due to a high intrinsic dielectric constant of crystallized TiO₂ (anatase, 30–40; rutile, 83–100) and the formation of perovskite crystal structure by the addition of A-site (Ba and/or Sr) cations [7, 8].

Among various thin film deposition techniques, atomic layer deposition (ALD) offers unique characteristics that make itself suitable for fabricating ultrathin dielectric films [9]. ALD is a modified chemical vapor deposition (CVD) technique, which is based on self-limiting surface reactions. Using ALD, one can deposit extremely uniform thin films conformally over high-aspect-ratio structured surfaces with sub-nm-level thickness control [10]. The thermal damage of the underlying

device can also be minimized due to the low process temperature (<400 °C) during ALD. In particular, plasma-enhanced ALD (PEALD), which utilizes highly reactive plasma species such as radicals or ions, offers greater process flexibility and a wider selection of materials than conventional thermal ALD. The plasma species are generally known to be beneficial in facile ligand exchange process that leads to low contamination inside films. It is also notable that the use of plasma in PEALD greatly enhances the film crystallinity that is crucial in device performance. Indeed, researchers at Stanford University have recently reported that the dielectric constant as well as the leakage current density of BTO or Al-doped BTO films can be greatly improved if they are better crystallized with a post-deposition remote oxygen plasma treatment in PEALD process [7, 8, 11].

While these recent works have examined the electrical and structural properties of PEALD-grown BTO thin films, their thermal properties remain to be investigated. This is particularly important because the thermal properties of high-dielectric-constant materials have become a key consideration for the implementation of these materials in high-performance electronic devices [12]. Unfortunately, however, there exist only a limited number of works that have reported the thermal properties of high-dielectric-constant materials deposited by ALD including ZrO₂ and HfO₂ [12–15]. In this work, we report the first measurements of the room temperature thermal conductivity of ultrathin (12 and 24 nm) BTO films deposited by PEALD. The thermal conductivities of as-deposited films are relatively low as compared to the data reported previously [16, 17]. Utilizing a remote oxygen plasma treatment

* Corresponding author.

** Correspondence to: J. An, Department of Manufacturing Systems and Design Engineering, Seoul National University of Science and Technology (SeoulTech), Seoul 01811, Republic of Korea

E-mail addresses: jungwan.cho@khu.ac.kr, (J. Cho), jihwanan@seoultech.ac.kr (J. An).

after deposition, we further proceed to study the effects of plasma-induced crystallization on the thermal conductivity of the PEALD BTO films. We find that the thermal conductivity of these films slightly decreases with increasing duration of plasma treatment and ascribe this to increased phonon scattering at interfaces between amorphous and crystalline phases within the films.

PEALD BTO films of 12 and 24 nm thicknesses were deposited in a commercial PEALD reactor (FlexAL, Oxford Instruments) with Ba ($i\text{Pr}_3\text{Cp}$)₂ (Air Liquide) and Ti(OCH(CH₃)₂)₄ (TTIP, Sigma Aldrich) as the Ba and Ti precursors, respectively, on highly p-doped Si wafers (a sheet resistance of 0.008 Ω cm). The deposition temperature was 250 °C. The temperature of Ba and Ti precursor canisters were heated at 180 and 55 °C, respectively. Oxygen plasma (plasma power, 250 W; operating pressure, 15 mTorr) was generated from an inductively coupled plasma system. PEALD BTO process is composed of 1 BaO cycle and 3 TiO₂ cycles. At the Ba:Ti cycle ratio of 1:3, the growth rate per supercycle (1 BaO cycle + 3 TiO₂ cycles) is 0.26 nm/cycle. Detailed sequences of BaO and TiO₂ cycles are described in the previous publication [8, 11]. After the BTO film deposition, samples were treated with the remote oxygen plasma (250 W, 15 mTorr) at 250 °C for 1 h and 3 h in the same PEALD chamber.

Fig. 1(a)–(c) show cross-sectional TEM images of as-deposited, 1 hr- and 3 hr-plasma treated PEALD BTO films, all of which are ~12 nm thick. The as-deposited film appears to be mostly amorphous with a few 1–2 nm nucleates (circled with yellow dotted lines) embedded within the film, which is not significantly different from thermal ALD BTO [7]. In contrast, the 1 hr-plasma treated film begins to show clearly crystallized regions (Fig. 1(b)), and the 3 hr-plasma treated film contains

a considerable portion of crystallized area in the film (Fig. 1(c)). The crystalline area fraction can be estimated from the TEM images taken at 4 different locations (Fig. 1(d)). The fraction of crystalline area increases as the film is exposed to longer plasma treatment: <1% in the as-deposited, $8 \pm 6\%$ in the 1 hr-plasma treated, and $22 \pm 12\%$ in the 3 hr-plasma treated films. Such plasma-induced crystallization of thin films has been reported previously [7, 18]. As described in these previous studies, we speculate that the ion bombardment on the film surface may have transferred the energy into the film to form nucleates even at the relatively low growth temperature (250 °C).

XPS measures Ba, Ti, and O contents to be 14.6 at%, 22.2 at%, and 62.8 at%, respectively (Fig. 2(a)), which means the BTO film is Ti-rich ($C_{\text{Ba}}/(C_{\text{Ti}} + C_{\text{Ba}}) \sim 0.40$). Little carbon content is detectable (<2 at%). XRR patterns in Fig. 2(b) further reveal the densities, thicknesses, and roughnesses of the 12 nm BTO films (Table S1). The densities of the as-deposited, 1 hr- and 3 hr-treated films are identical with each other (4.92–4.95 g/cm³). Considering the mixed crystallinity, i.e., partially crystalline regions embedded within an amorphous matrix, of our films, such measured densities are in accordance with the previously reported density values of BTO (amorphous 4.30 g/cm³, polycrystalline 5.61 g/cm³, single-crystal 6.02 g/cm³) [19]. The densification of BTO films by post-deposition plasma treatment, which has been observed in thermal ALD BTO films [7], is not clearly shown possibly due to the already dense nature of our as-deposited PEALD BTO films. The film thickness does not change significantly despite prolonged plasma treatment (12.0–12.2 nm). The surfaces of all the films are very smooth (RMS roughness of 0.75–0.83 nm).

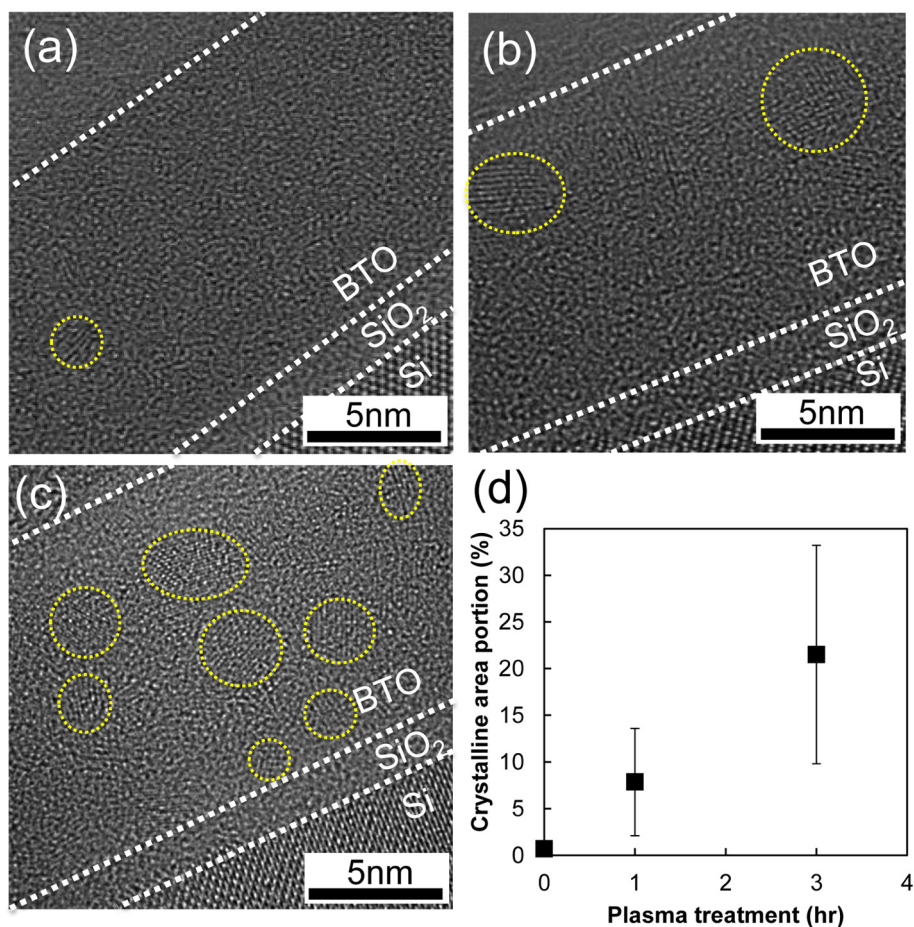


Fig. 1. Cross-sectional TEM images of PEALD BTO films: (a) as-deposited, (b) after 1 hr treatment, and (c) after 3 hr post-deposition treatment of oxygen plasma. Crystallized regions are marked with yellow dotted lines. (d) Crystalline area fraction vs. post-deposition plasma treatment duration determined by TEM images (based on 4 different images for each data point).

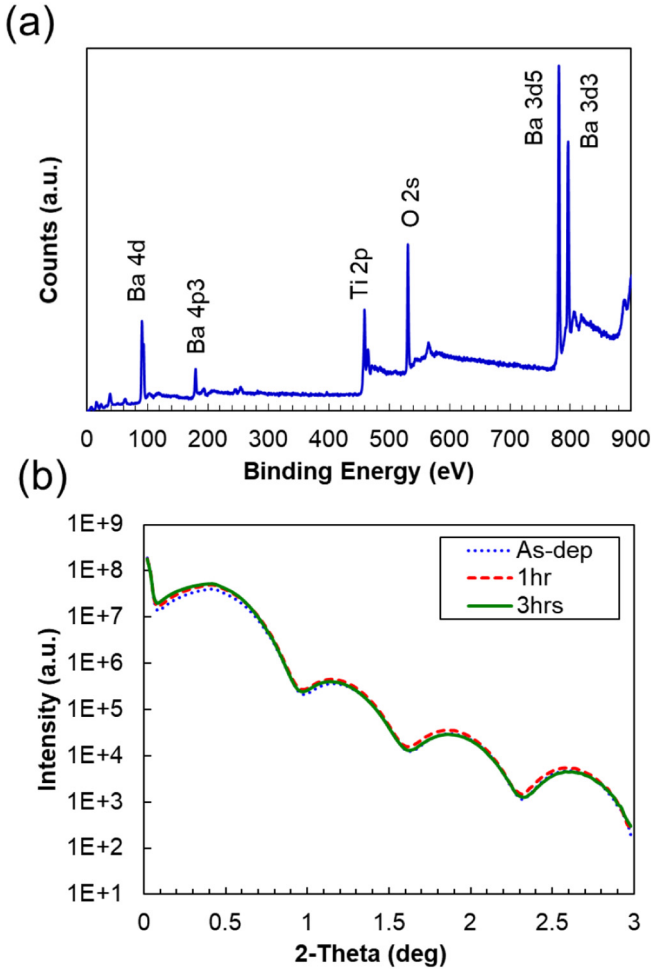


Fig. 2. (a) XPS spectra of as-deposited PEALD BTO and (b) XRR patterns for as-deposited, 1 hr, and 3 hr-treated PEALD BTO films.

Time-domain thermoreflectance (TDTR) measures the thermal conductivity of the PEALD BTO films [20–24]. An ~51 nm Al film that acts as a transducer layer is electron-beam evaporated on the surface of the BTO films for TDTR measurements. For our BTO samples, there are three unknown parameters that are obtained by fitting the multilayer thermal model to the TDTR data with a nonlinear least-squares curve-fitting algorithm. These are i) the TBR at the Al/BTO interface (TBR_{Al-BTO}), ii) the thermal conductivity of the BTO layer (k_{BTO}), and iii) the

(total) TBR at the BTO/SiO₂/Si interface (TBR_{BTO-Si}). All other parameters except these three are given as an input to the model. More details of the TDTR experiment and corresponding thermal analysis can be found in the supplementary material.

The TDTR measurement sensitivity is standardly defined as $S_{\beta} = \partial \ln(R) / \partial \ln(\beta)$ [21–24], where R is the TDTR signal (in this study, it's the amplitude $\sqrt{V_{in}^2 + V_{out}^2}$ of the in-phase and out-of-phase temperature signals) and β is the parameter of interest in the multilayer thermal model. As a representative example, Fig. 3 shows the sensitivity to the three unknown parameters (TBR_{Al-BTO} , k_{BTO} , TBR_{BTO-Si}) for the 12 nm 3 hr-plasma treated BTO sample and the 24 nm 3 hr-plasma BTO sample as a function of pump-probe delay time and at the 6 MHz pump modulation frequency. For the sensitivity calculations in Fig. 3, we assume TBR_{BTO-Si} to be the median of a range from 2 to 9 m² K GW⁻¹ (which is discussed later), and use best-fit values for TBR_{Al-BTO} and k_{BTO} . Representative TDTR data along with optimal theoretical fits are shown in Fig. S1.

As illustrated in Fig. 3(a), we are most sensitive to k_{BTO} , while less sensitive to TBR_{Al-BTO} and TBR_{BTO-Si} for the 12 nm samples. But the magnitudes of the sensitivity to TBR_{Al-BTO} and TBR_{BTO-Si} for these samples are not negligible as compared to those to k_{BTO} (e.g., $|S_{k_{BTO}}| \sim 0.40$ vs. $|S_{TBR_{BTO-Si}}| \sim 0.12$, $|S_{TBR_{Al-BTO}}| \sim 0.07$ at 3.5 ns in Fig. 3(a)), and the sensitivity curves of TBR_{Al-BTO} , k_{BTO} , and TBR_{BTO-Si} are similar in shape over the entire range of delay time. This implies that the TDTR measurement for the three 12 nm samples is not able to uniquely separate these three parameters [25]. Instead, the measurement is only sensitive to the total summed resistance R_T that combines the volumetric resistance of the BTO layer ($R_{BTO} = d_{BTO}/k_{BTO}$, where d_{BTO} is the BTO layer thickness) and the two boundary resistances at the top and bottom BTO layer boundaries (TBR_{Al-BTO} , TBR_{BTO-Si}): $R_T = TBR_{Al-BTO} + R_{BTO} + TBR_{BTO-Si}$. Thus, for the three 12 nm samples, we sum the resulting fitted values of TBR_{Al-BTO} , R_{BTO} , and TBR_{BTO-Si} —which do not have meaning individually for this specific set of samples—to calculate R_T . We find R_T to be 20.7 ± 2.0 , 23.0 ± 2.2 , and 27.2 ± 3.0 m² K GW⁻¹ for the as-deposited, 1 hr- and 3 hr-treated samples, respectively. If we convert R_T to an effective thermal conductivity of the BTO film ($k_{BTO, eff} = d_{BTO}/R_T$), then we obtain 0.59 ± 0.06 , 0.53 ± 0.06 , and 0.44 ± 0.05 W m⁻¹ K⁻¹ for the as-deposited, 1 hr- and 3 hr-treated samples, respectively.

As a next step, we utilize thicker BTO samples (i.e., approximately 24 nm as-deposited, 1 hr-plasma-treated, and 3 hr-plasma-treated ones) to increase the measurement sensitivity to k_{BTO} relative to those to TBR_{Al-BTO} and TBR_{BTO-Si} . Fig. 3(b) demonstrates that for these samples the sensitivity to k_{BTO} is dominant over those to TBR_{Al-BTO} and TBR_{BTO-Si} (e.g., $|S_{k_{BTO}}| \sim 0.37$ vs. $|S_{TBR_{Al-BTO}}| \sim 0.04$, $|S_{TBR_{BTO-Si}}| \sim 0.07$ at 3.5 ns). This allows us to separate the BTO thermal conductivity from

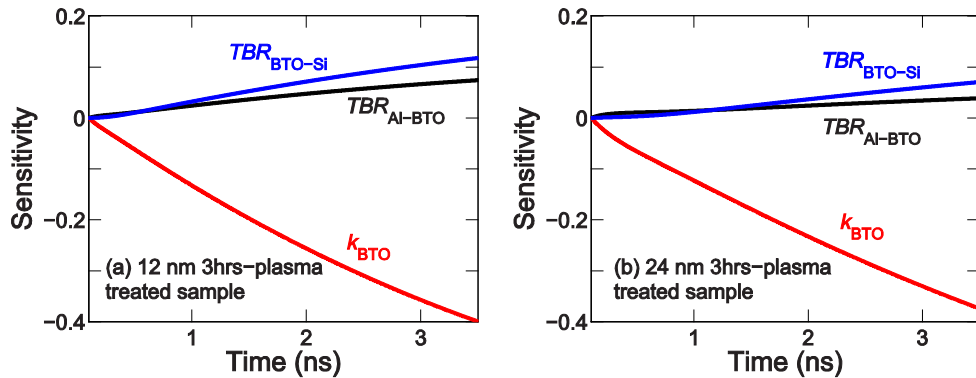


Fig. 3. TDTR sensitivity to the Al/BTO thermal boundary resistance TBR_{Al-BTO} (black), the BTO thermal conductivity k_{BTO} (red), and the BTO/Si thermal boundary resistance TBR_{BTO-Si} (blue) for (a) the 12 nm 3 hr-plasma treated sample and (b) the 24 nm 3 hr-plasma treated sample as a function of pump-probe delay time at a pump modulation frequency of 6 MHz. Large magnitude of the sensitivity to k_{BTO} , relative to those to TBR_{Al-BTO} and TBR_{BTO-Si} , demonstrates that our measurements are most sensitive to k_{BTO} for both samples.

the other two parameters. For $TBR_{\text{BTO-Si}}$, we assume a range of values from 2 to 9 $\text{m}^2 \text{K GW}^{-1}$, which is consistent with the range reported in literature for dielectric/native oxide/Si interfaces [12, 13]. We fit the TDTR data with k_{BTO} and $TBR_{\text{Al-BTO}}$ as two adjustable parameters, while fixing $TBR_{\text{BTO-Si}}$ at the median of the range assumed here. The lower bound of $TBR_{\text{BTO-Si}}$ is estimated to be 2 $\text{m}^2 \text{K GW}^{-1}$ by summing the volumetric resistance of the $\sim 1.4 \text{ nm}$ SiO_2 interlayer (assuming $1.4 \text{ W m}^{-1} \text{K}^{-1}$ for the SiO_2 thermal conductivity) and the boundary resistance at direct BTO/Si contact (without SiO_2 interlayer). The latter is predicted by using a modified version of the diffuse mismatch model that considers the actual phonon density of states in materials via the measured heat capacity data [26, 27]. We estimate the upper bound of $TBR_{\text{BTO-Si}}$ to be 9 $\text{m}^2 \text{K GW}^{-1}$ by subtracting the volumetric resistance of the 12 nm BTO layer—with the BTO thermal conductivity taken from the previous data for a polycrystalline 175 nm BTO film with a grain size of 36 nm ($1 \text{ W m}^{-1} \text{K}^{-1}$) [17]—from the measured total thermal resistance of the 12 nm as-deposited sample ($\sim 21 \text{ m}^2 \text{K GW}^{-1}$). The uncertainty in $TBR_{\text{BTO-Si}}$ —owing to the range assumed here—propagates to uncertainties in k_{BTO} of 20, 12, and 11% for the as-deposited, 1 hr- and 3 hr-treated samples, respectively. Our analysis yields the BTO thermal conductivity of 1.10 ± 0.25 , 0.97 ± 0.15 , and $0.92 \pm 0.14 \text{ W m}^{-1} \text{K}^{-1}$ for the as-deposited, 1 hr- and 3 hr-treated samples, respectively.

The uncertainties in our reported values for all the samples with both thicknesses are calculated by propagating uncertainties in the Al thickness and thermal conductivity, the BTO layer thickness, and the thermal conductivity of the Si substrate, as well as the boundary resistance at the BTO/Si interface.

Fig. 4 shows the measured thermal conductivities of our BTO films as a function of plasma treatment duration. As discussed above, the data for the three 12 nm BTO samples represent the effective thermal conductivity that includes the contributions from the boundary resistances ($TBR_{\text{Al-BTO}}$, $TBR_{\text{BTO-Si}}$), as well as the volumetric BTO resistance, while the data for the three 24 nm BTO samples represent the BTO thermal

conductivity that is separated from the two boundary resistances. This explains the lower conductivity values observed in the thinner films. For comparison, Fig. 4 includes the data for the room-temperature thermal conductivity of bulk single crystal BTO ($5.7 \text{ W m}^{-1} \text{K}^{-1}$) [16] and polycrystalline 175 nm BTO films, prepared by chemical solution deposition (CSD), with average grain sizes of 36 and 63 nm (1.0 and $1.7 \text{ W m}^{-1} \text{K}^{-1}$, respectively) [17].

The thermal conductivity of our 24 nm as-deposited PEALD BTO film ($1.1 \text{ W m}^{-1} \text{K}^{-1}$) is close to the lower end of the range reported previously for the CSD BTO films (1.0 – $1.7 \text{ W m}^{-1} \text{K}^{-1}$) [17]. One possible explanation is due to the amorphous nature of our as-deposited films [28]. A second possibility is the effects of phonon scattering on film and grain boundaries [17, 29]. Our films are thinner than both the film thickness and grain sizes of the CSD films. Given that the limiting dimension of the films is the film thickness in our films and the grain size in the CSD films, boundary scattering limited transport may explain the data trend observed in our films and the CSD films. A third possibility is that our films are Ti-rich, which could also lead to increased phonon scattering from point defects [30]. A fourth possibility is owing to a potential role played by density. Although the film densities were not reported for the CSD films [17], previous works have demonstrated the density dependence of the thermal conductivity of ALD-grown amorphous TiO_2 and Al_2O_3 thin films [25, 31].

The data for both the 12 and 24 nm samples exhibit the trend that the thermal conductivity slightly decreases with increasing duration of plasma treatment. The reduction observed in thermal conductivity is most likely due to the increased nanocrystalline volume fraction and associated increase in interface resistance (between crystalline and amorphous phases) with longer duration of plasma treatment [13, 32–34]. The increased scattering of phonons at these crystalline/amorphous interfaces may be responsible for such an increase in the interface resistance, which may be larger than the possible reduction in the volumetric BTO resistance owing to the increased crystalline volume fraction [13, 34]. Previous works have reported similar reductions in the thermal conductivity of approximately 6–20 nm ALD HfO_2 films with increasing crystalline volume fraction [13] and of $\text{In}_{0.53}\text{Ga}_{0.47}\text{As}$ samples with increasing ErAs nanoparticle concentration [35].

This work presents the first experimental investigation of the thermal conductivity of ultrathin (12 and 24 nm) PEALD BTO films using TDTR. The as-deposited films show a reduced thermal conductivity, compared with bulk single crystal BTO and polycrystalline BTO films with grain sizes of 36–63 nm. A remote oxygen plasma treatment after deposition crystallize these films, as evident by the comparison of the morphological features between as-deposited and plasma-treated films. We observe that the thermal conductivity of our BTO films is slightly reduced with longer exposure to oxygen plasma, which can be ascribed most likely to increased phonon scattering at interfaces between crystalline and amorphous phases within the films.

Notes

Experimental details, including the TDTR experiment, are described in the Supplementary material. The authors declare no competing financial interest.

Acknowledgment

This work was supported by the National Research Foundation of Korea (NRF) grants funded by the Korea government (MSIP) (No. 2016R1C1B2015317, No. 2017M1A3A3A02016562 and No. NRF-2018R1C1B6001150).

Appendix A. Supplementary data

Supplementary data to this article can be found online at <https://doi.org/10.1016/j.scriptamat.2018.05.049>.

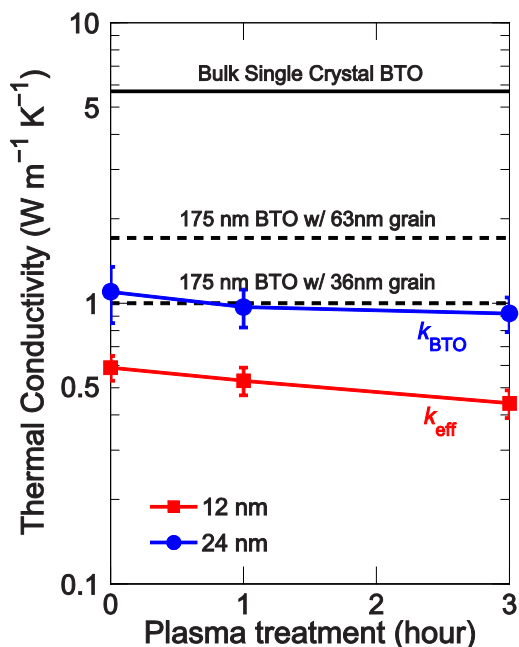


Fig. 4. Thermal conductivity of PEALD BTO films as a function of duration of plasma treatment. Red square markers represent the effective thermal conductivity for three 12 nm samples, and blue circle markers represent the BTO thermal conductivity for three 24 nm samples. Also shown are the previous data for polycrystalline 175 nm BTO films (prepared by chemical solution deposition) with average grain sizes of 36 and 63 nm (two black dashed lines) [17] and bulk single crystal BTO (black solid line) [16].

References

- [1] A.I. Kingon, J.-P. Maria, S.K. Streiffer, *Nature* 406 (2000) 1032.
- [2] M. Seo, S.K. Kim, J.H. Han, C.S. Hwang, *Chem. Mater.* 22 (2010) 4419.
- [3] M. Vehkamäki, T. Hatanpää, T. Hänninen, M. Ritala, M. Leskelä, *Electrochem. Solid-State Lett.* 2 (1999) 504.
- [4] Z. Wang, T. Yasuda, S. Hatatani, S. Oda, *Jpn. J. Appl. Phys.* 38 (1999) 6817.
- [5] S.W. Lee, O.S. Kwon, J.H. Han, C.S. Hwang, *Appl. Phys. Lett.* 92 (2008) 222903.
- [6] R. Schafrank, A. Giere, A.G. Balogh, T. Enz, Y. Zheng, P. Scheele, R. Jakoby, A. Klein, *J. Eur. Ceram. Soc.* 29 (2009) 1433.
- [7] J. An, T. Usui, M. Logar, J. Park, D. Thian, S. Kim, K. Kim, F.B. Prinz, *ACS Appl. Mater. Interfaces* 6 (2014), 10656.
- [8] Y. Kim, P. Schindler, A.L. Dadlani, S. Acharya, J. Provine, J. An, F.B. Prinz, *Acta Mater.* 117 (2016) 153.
- [9] S.M. George, *Chem. Rev.* 110 (2009) 111.
- [10] P. Schindler, M. Logar, J. Provine, F.B. Prinz, *Langmuir* 31 (2015) 5057.
- [11] P. Schindler, Y. Kim, D. Thian, J. An, F.B. Prinz, *Scr. Mater.* 111 (2016) 106.
- [12] J.T. Gaskins, P.E. Hopkins, D.R. Merrill, S.R. Bauers, E. Hadland, D.C. Johnson, D. Koh, J.H. Yum, S. Banerjee, B.J. Nordell, M.M. Paquette, A.N. Caruso, W.A. Lanford, P. Henry, L. Ross, H. Li, L. Li, M. French, A.M. Rudolph, S.W. King, *ECS J. Sol. State Sci. Technol.* 6 (2017) N189.
- [13] M.A. Panzer, M. Shandalov, J.A. Rowlette, Y. Oshima, Y.W. Chen, P.C. McIntyre, K.E. Goodson, *IEEE Electron Device Lett.* 30 (2009) 1269.
- [14] N.T. Gabriel, J.J. Talghader, *J. Appl. Phys.* 110 (2011), 043526.
- [15] J. Cho, J. Park, J. An, J. Eur. Ceram. Soc. 37 (2017) 3131.
- [16] A.J.H. Mante, J. Volger, *Phys. Lett. A* 24 (1967) 139.
- [17] B.F. Donovan, B.M. Foley, J.F. Ihlefeld, J.-P. Maria, P.E. Hopkins, *Appl. Phys. Lett.* 105 (2014), 082907.
- [18] J. Kim, S. Kim, H. Jeon, *Appl. Phys. Lett.* 87 (2005), 053108.
- [19] E.T. Ryan, J. Martin, K. Junker, J. Wetzal, D.W. Gidley, J.N. Sun, *J. Mater. Res.* 16 (2001) 3335.
- [20] D.G. Cahill, *Rev. Sci. Instrum.* 75 (2004) 5119.
- [21] A.J. Schmidt, X. Chen, G. Chen, *Rev. Sci. Instrum.* 79 (2008) 114902.
- [22] D.G. Cahill, P.V. Braun, G. Chen, D.R. Clarke, S. Fan, K.E. Goodson, P. Keblinski, W.P. King, G.D. Mahan, A. Majumdar, H.J. Maris, S.R. Phillpot, E. Pop, L. Shi, *Appl. Phys. Rev.* 1 (2014), 011305.
- [23] J. Cho, Y. Li, W.E. Hoke, D.H. Altman, M. Asheghi, K.E. Goodson, *Phys. Rev. B* 89 (2014) 115301.
- [24] A. Sood, J. Cho, K.D. Hobart, T.I. Feyselson, B.B. Pate, M. Asheghi, D.G. Cahill, K.E. Goodson, *J. Appl. Phys.* 119 (2016), 175103.
- [25] M.E. DeCoster, K.E. Meyer, B.D. Piercy, J.T. Gaskins, B.F. Donovan, A. Giri, N.A. Strnad, D.M. Potrepka, A.A. Wilson, M.D. Losego, P.E. Hopkins, *Thin Solid Films* 650 (2018) 71.
- [26] L.D. Bellis, P.E. Phelan, R.S. Prasher, *J. Thermophys. Heat Transf.* 14 (2000) 144.
- [27] J. Cho, D. Francis, D.H. Altman, M. Asheghi, K.E. Goodson, *J. Appl. Phys.* 121 (2017), 055105.
- [28] D.G. Cahill, S.K. Watson, R.O. Pohl, *Phys. Rev. B* 46 (1992) 6131.
- [29] A.M. Marconnet, M. Asheghi, K.E. Goodson, *J. Heat Transf.* 135 (2013), 061601.
- [30] B.F. Donovan, D.M. Long, A. Moballeggh, N. Creange, E.C. Dickey, P.E. Hopkins, *Acta Mater.* 127 (2017) 491.
- [31] C.S. Gorham, J.T. Gaskins, G.N. Parsons, M.D. Losego, P.E. Hopkins, *Appl. Phys. Lett.* 104 (2014), 253107.
- [32] J. Lee, Z. Li, J.P. Reifenberg, S. Lee, R. Sinclair, M. Asheghi, K.E. Goodson, *J. Appl. Phys.* 109 (2011), 084902.
- [33] Z. Li, J. Lee, J.P. Reifenberg, M. Asheghi, R.G. Jeyasingh, H.P. Wong, K.E. Goodson, *IEEE Electron Device Lett.* 32 (2011) 961.
- [34] B.T. Kearney, B. Jugdersuren, D.R. Queen, T.H. Metcalf, J.C. Culbertson, P.A. Desario, R.M. Stroud, W. Nemeth, Q. Wang, X. Liu, *J. Phys. Condens. Matter* 30 (2018), 085301.
- [35] W. Kim, J. Zide, A. Gossard, D. Klenov, S. Stemmer, A. Shakouri, A. Majumdar, *Phys. Rev. Lett.* 96 (2006), 045901.